



HAL
open science

Encoding information onto the charge and spin state of a paramagnetic atom using MgO tunnelling spintronics

Mathieu Lamblin, Bhavishya Chowrira, Victor da Costa, Bertrand Vilen, Loic Joly, Samy Boukari, Wolfgang Weber, Romain Bernard, Benoit Gobaut, Michel Hehn, et al.

► To cite this version:

Mathieu Lamblin, Bhavishya Chowrira, Victor da Costa, Bertrand Vilen, Loic Joly, et al.. Encoding information onto the charge and spin state of a paramagnetic atom using MgO tunnelling spintronics. 2023. hal-04274716

HAL Id: hal-04274716

<https://hal.science/hal-04274716>

Preprint submitted on 8 Nov 2023

HAL is a multi-disciplinary open access archive for the deposit and dissemination of scientific research documents, whether they are published or not. The documents may come from teaching and research institutions in France or abroad, or from public or private research centers.

L'archive ouverte pluridisciplinaire **HAL**, est destinée au dépôt et à la diffusion de documents scientifiques de niveau recherche, publiés ou non, émanant des établissements d'enseignement et de recherche français ou étrangers, des laboratoires publics ou privés.



Distributed under a Creative Commons Attribution - NonCommercial 4.0 International License

Encoding information onto the charge and spin state of a paramagnetic atom using MgO tunnelling spintronics

Mathieu Lamblin,^{1, a)} Bhavishya Chowrira,¹ Victor Da Costa,¹ Bertrand Vilenó,² Loïc Joly,¹ Samy Boukari,¹ Wolfgang Weber,¹ Romain Bernard,¹ Benoit Gobaut,¹ Michel Hehn,³ Daniel Lacour,³ and Martin Bowen¹

¹⁾*Institut de Physique et Chimie des Matériaux de Strasbourg, UMR 7504 CNRS, Université de Strasbourg, 23 Rue du Læss, BP 43, 67034 Strasbourg, France*

²⁾*Institut de Chimie UMR 7177 CNRS Université de Strasbourg 4 Rue Blaise Pascal, CS 90032, Strasbourg 67081, France*

³⁾*Institut Jean Lamour UMR 7198 CNRS Université de Lorraine BP 70239, Vandoeuvre les Nancy 54506, France*

(Dated: September 1, 2023)

An electrical current that flows across individual atoms or molecules can generate exotic quantum-based behavior, from memristive effects to Coulomb blockade and the promotion of quantum excited states. These fundamental effects typically appear one at a time in model junctions built using atomic tip or lateral techniques. So far, however, a viable industrial pathway for such discrete state devices has been lacking. Here, we demonstrate that a commercialized device platform can serve as this industrial pathway for quantum technologies. We have studied magnetic tunnel junctions with a MgO barrier containing C atoms. The paramagnetic localized electrons due to individual C atoms generate parallel nanotransport paths across the micronic devices deduced from magnetotransport experiments. Coulomb blockade effects linked to tunnelling magnetoresistance peaks can be electrically controlled, leading to a persistent memory effect. Our results position MgO tunneling spintronics as a promising platform to industrially implement quantum technologies.

Research on model atomic and molecular junctions has strongly progressed in the last two decades thanks to atomic tip and lateral junction building techniques. These technological advancements have helped reveal intriguing transport mechanisms, such as Coulomb blockade inside single-atom transistors¹, Coulomb drag and co-tunneling effects in capacitively coupled quantum dots², Franck-Condon blockade within carbon nanotubes³, spin-phonon coupling in single-molecule magnets⁴, Kondo effect with spin-oriented molecules⁵, memristance and hysteresis linked to resistive switching^{6,7} and strong current fluctuations caused by vibrational coupling and structural changes⁸. More recently, quantum phenomena involving internal coherence and superposition have been reported, such as phonon interference⁹, quantum interference and decoherence¹⁰.

If ferromagnetic electrodes are used to establish a fixed spin referential, then the resulting spintronic device can better exploit the electron spin to encode quantum information¹¹ or harvest thermal energy using discrete spin states^{12,13}. While molecules offer elegant means of inserting discrete electronic states within a device, molecular spintronic strategies are still far from industrial deployment^{11,14}.

Finally, much research has focused on transposing robust state changes to a junction's spintronic response from more exotic barriers such as SrTiO₃¹⁵ to the most widely developed industrial spintronic platform: the FeCoB/MgO/FeCoB magnetic tunnel junction (MTJ), with applications ranging from next-generation

memories¹⁶ and neuromorphic computing¹⁷ to agile microwave emitters and artificial energy harvesting¹⁸.

In this paper, we demonstrate several of the aforementioned quantum effects using the industrialization vector that is MgO tunnelling spintronics. Prior literature on MgO tunnelling indicates that structural defects can generate localized states within the tunnel barrier^{19–23}. The tunnel barrier's oxygen vacancies generate discrete electronic states that we have identified²³ and controlled²⁴ in our MgO junctions. These oxygen vacancies are diamagnetic. To achieve discrete, unpaired electron spin states, we introduce carbon atoms onto these oxygen vacancies¹² (see Methods).

We observe that microscale MTJs with C atoms in the MgO barrier can exhibit noise and two/multi-level states of electrical transport (see Methods for technological processing). We now present evidence that the C-borne spin states can be electrically manipulated to encode information. The cyclical IV traces of junction G10 in Fig. 1(a) show two current branches that are linked through events E_- and E_+ . Between these two events, the ON branch is represented in black while the OFF branch is in red. In Fig. 1(b) the corresponding set of differential conductance (dI/dV) is represented. We witness the presence of two conductance peaks at bias positions that depend on the direction of the voltage sweep. In the ON branch, they manifest around $V = V_+^{ON}$ and $V = V_-^{ON}$, and they are shifted by $\Delta_W \approx 70$ mV compared with the OFF branch. As discussed in SI Note 4, the constant voltage gap $\Delta_{CG} = 300$ mV between the pair of conductance peaks can be tracked across several other states of the junction G10. Within this voltage gap, we observe an exponential increase in junction current. We therefore propose that these conductance peaks correspond to the

^{a)}Electronic mail: mathieu.lamblin@ipcms.unistra.fr

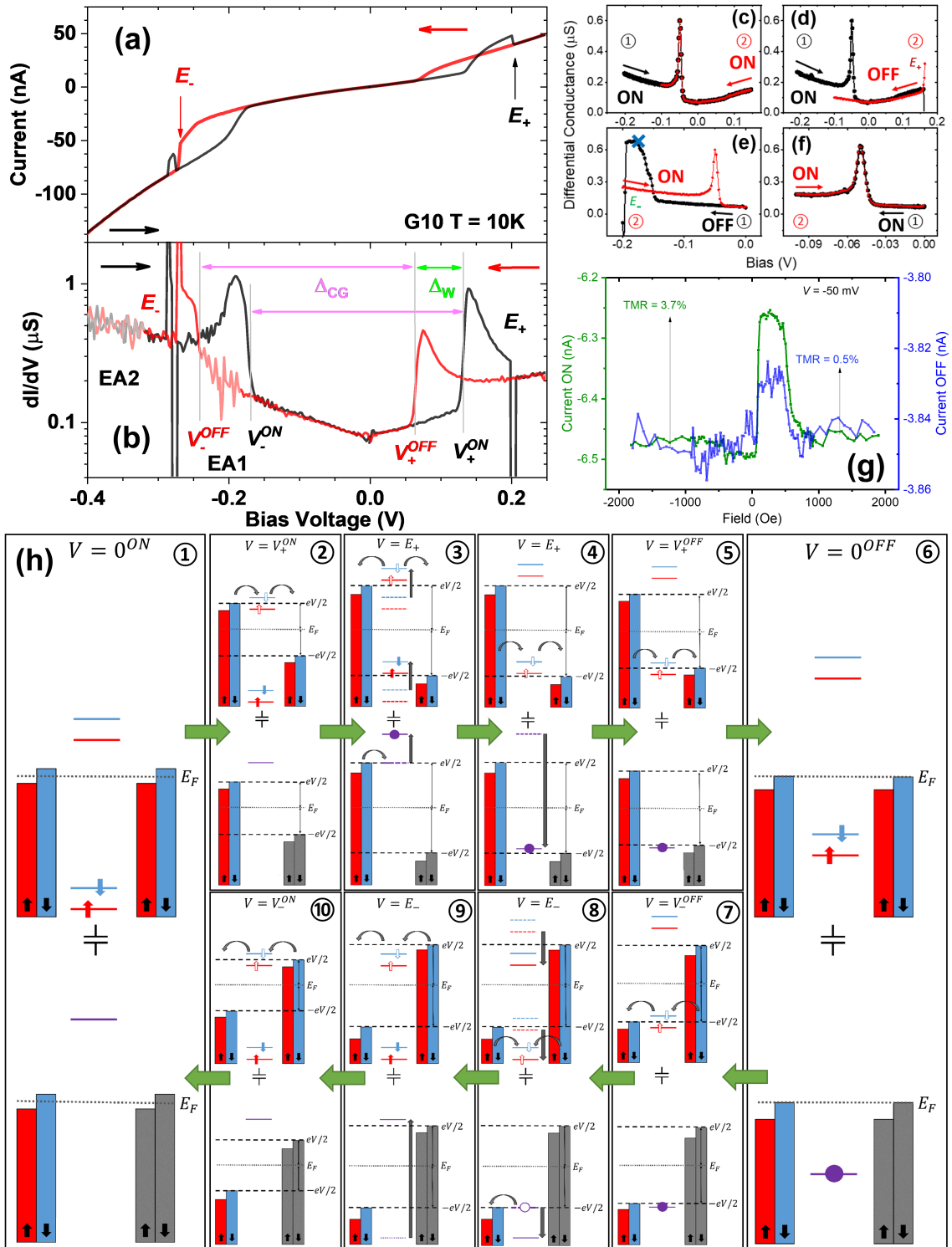



Figure 1. **Memristive Coulomb blockade at the atomic level.** (a) IV and (b) differential conductance dI/dV data at $T = 10$ K on junction G10. The E_+ and E_- writing events cause a shift $\Delta_W = 73$ mV in the otherwise constant energy gap $\Delta_{CG} = 310$ mV between conductance peaks. Transport noise due to interference with an environmental atom are shown using semi-transparent datapoints (c-f) dI/dV data upon sweeping bias to test the interplay between the presence of the Coulomb blockade peak and the writing events E_- and E_+ . The black data labeled 1 code for the initial branch state of the junction, then the sweep direction is inverted and the return branch is represented in red and labeled 2. The blue cross in panel (e) pinpoint the bias and junction state in which the data of Fig. 2(a) was acquired. (g) Magnetoresistance traces at $V = -50$ mV in the ON/OFF junction states. (h) Model of a memristive Coulomb blockade involving at least one atom in the transport path, and at least one 'environmental' atom that is capacitively linked to the transport atom but doesn't participate directly in electronic transport across the junction. The various operations of the memristive cycle, showing how charging/discharging the environmental atom controls the energy levels of the transport atom, are shown.

edges of the Coulomb blockade regime across the MgO MTJ thanks to electronic states of C atoms in the MgO barrier. We also propose that the shift in the energy position of the Coulomb gap be the result of charging on 'environmental' C atoms that do not participate in transport. This is supported in Fig. 1(a) by the presence of noisy regions EA1 and EA2 (semi-transparent data-points). Indeed, the spectral position and width of these regions do not correspond to Coulomb blockade peaks in the present dataset, but rather in other datasets acquired on the same junction but with different 'transport' and 'environmental' attributions of the C atoms.  SI Note 4 for details.

To obtain atomic insight into the nanojunction's nanotransport path, we use $\Delta_{CG} = 300$ mV as a lower bound for the Coulomb gap of the 'transport' quantum dot generated by the carbon atoms. Using an appropriate capacitance model, this allows us to estimate a 0.2 nm radius for the transport quantum dot (see SI Note 5), i.e. approximately one monolayer of MgO. This large Coulomb gap thus indicates that transport is proceeding across the electronic states of an individual carbon atom. Furthermore, if the voltage shift $\Delta_W \approx 70$ mV between junction states corresponds to changing the environmental atom's charge by 1 electron, then we infer that it is positioned at twice the radius away from the 'transport' C atom (see SI Note 5).

The nanotransport path thus consists of at least one C atom, which is capacitively coupled to a nearby 'environmental' C atom. Our survey of Coulomb blockade peaks (see SI Note 4) suggests that several C atoms can be in the transport path, and that a given atom may switch between 'transport' and 'environmental' roles depending on the atomic-level configuration of the nanotransport at each junction cooldown.

To prove that events E_- and E_+ indeed code the shift of the Coulomb blockade peaks, we present in panels (c)-(f) of Fig. 1 the dI/dV traces from different IV paths in which we revert the voltage sweep direction just before and just after the events E_- and E_+ . For each panel, the initial state of the junction is coded as '1', the color black and the arrow pointing towards the sweep direction. Once the sweep is inverted, the return state is presented in red and coded by the number 2. In panel (c), when in the ON state and starting at a low bias value, if the bias is increased so as to sweep through the Coulomb blockade peak (black data) but remain below the E_+ event, the return sweep (red data) reproduces the Coulomb blockade peak. In this scenario, if the E_+ event is reached, then the return trace shows no Coulomb blockade peak so the junction has switched to the OFF state and the peak encoding information has been erased (panel (d)). Similarly, when in the ON state and the branch 1 sweeps from above the Coulomb blockade peak without reaching the E_- event, the peak readout is unchanged (panel (f)). Panel (e) however shows how, starting from the OFF state, reaching event E_- causes the junction to revert to the ON state, characterized by the bit coded by

the Coulomb blockade peak, which shows that the event E_- indeed corresponds to the writing.

Given the low electric field amplitude and the ionic nature of MgO, an explanation of events E_- and E_+ in terms of electromigration of oxygen vacancies is very unlikely²⁵. Indeed, the ionic bonding of the MgO lattice makes it difficult for oxygen vacancies and other on-site defects to move within the crystal structure at room temperature and below²⁶. Therefore, the observed resistive switching cannot be attributed to the migration of O^{2-} ions as this is frequently the case in other oxides such as NiO²⁷. It is possible, however, that an electromigration scenario be more favorable if the oxygen vacancies are filled²⁶ as is the case here.

Nevertheless, analogous hysteretic behavior induced by conductance jumps have been reported in molecular junctions²⁸⁻³⁰ and scanning tunneling microscopy experiments³¹⁻³⁴ but we now have showed that this phenomenon can also be observed in standard oxide-based junctions. The abrupt switching between two conductance branches results from a charging mechanism similar to the effect reported by Wu *et al.*³¹. Their results corroborate very well with our description featuring at least one control 'environmental' atom, whose charge can be directly tuned by the voltage, which in return capacitively influences the energy landscape of the 'transport' atom, as a gate voltage would control the current flow in single-electron transistors. In chemical words, the oxidation or reduction of the trapped C atom acting as the control quantum dot changes the nanotransport path taken by the electrons, which translates into different intensity branches.

We present in Fig. 1(h) the schematic of a two-atom model that can explain this memristive Coulomb blockade behavior. We consider two quantum dots: the upper one is the 'transport' quantum dot (TQD) and is connected to both leads, while the lower one is 'environmental' or 'control' quantum dot (EQD) and is connected only to the left lead. Both quantum dots are capacitively coupled together.

Starting at $V = 0$ in the OFF branch, the lower lying levels of the TDQ are filled, the upper lying are empty, and the single level of the EQD is empty (see Fig. 1(h)1). By increasing the voltage, a first conductance peak is seen on the dI/dV plot around $V = V_+^{ON}$ which corresponds to the upper edge of the Coulomb blockade region. The potential of the left lead is approaching the upper level of the TDQ, allowing for the start of sequential tunneling (see Fig. 1(h)2). By increasing the voltage to $V = E_+$, the potential of the left electrode aligns with the level of the EQD. A single electron can thus jump from the electrode to this level, which has the effect of lifting up the levels of both QDs in a first round. The upper lying levels of the TQD are now above the potential, while the lower levels rise between the potential window offered by the electrodes (see Fig. 1(h)3). During a second round, after equilibration, the electrons tunnel out of the TQD higher levels and sequential tunneling starts through the lower

levels. The new dynamic filling of the energy levels of the TQD act capacitively in return on the EQD, which has the effect of lowering its level (see Fig. 1(h)4). Therefore, this capacitive back action traps the electron that filled the EQD level, preventing it from jumping back into the electrode. A conductance jump from the ON branch to the OFF branch is thus observed in this case and we can see that the potential will have to decrease to negative values in order to remove this trapped electron and revert back to the ON state.

From this unstable state in Fig. 1(h)3, the system can either go back to configuration 2 if the reverse jump process happens, or it can switch to the next transport regime if the filling of the transport atom changes because of this capacitive interaction. Hence, there is a small bias window in which the system can eventually fluctuate between two states before it stabilizes when the electron/-dot on the environmental atom gets trapped as a result of a favorable capacitive coupling. The intensity of the fluctuation is driven by the ratio between the hopping frequencies of the environmental dot by the transport dot. If the jump frequency of the tunnelling processes on the TQD is much higher than that on the EQD, then the equilibration of the TQD will happen before any reverse jump can occur on the EQD, resulting in a single branch jump.

If the voltage is now decreased, another conductance peak is observed around $V = V_+^{OFF}$ which corresponds this time to the end of sequential tunneling through the lower lying level of the TQD (see Fig. 1(h)5). Going back to $V = 0$, the Coulomb blockade region is recovered but the levels of the TDQ are now arranged differently because of the presence of the electron in the EQD level (see Fig. 1(h)6). When the bias is decreased to negative values, sequential tunneling can start again through the lower levels of the TDQ around $V = V_-^{OFF}$ (see Fig. 1(h)7). Approaching $V = E_-$, the potential of the left electrode now aligns again with the EQD level, allowing for the trapped electron to jump back into the lead. This change of charge borne by the EQD lowers the levels of QDs. Similarly, the upper levels are now located inside the potential window, while the lower levels are shifted below the potential of both electrodes, so they must be filled to reach equilibrium (see Fig. 1(h)8). This triggers a second round of effects where sequential tunneling now goes through the upper lying levels, while the lower lying levels stay filled. This change of electronic environment of the TQD acts again capacitively on the EQD, lifting up the energy level (see Fig. 1(h)9). The removing of the trapped electron thus triggers a branch jump from the OFF branch back to the ON branch. By increasing the potential, a final conductance peak is observed around $V = V_-^{ON}$ which corresponds to the end of sequential tunneling through the upper lying level of the TQD (see Fig. 1(h)10). The cycle is completed at $V = 0$ where the junction has indeed returned to the ON branch (see Fig. 1(h)1).

Close to $V = E_-$, we notice that several branch jumps

between the ON and OFF branches can occur. This behaviour is qualitatively expected by our schematics which can describe several jumps at this potential, resulting from multiple electron processes but the precise mechanisms that triggers these transitions remain to be detailed. We infer that at this special bias, the position of the energy levels is such that cotunneling phenomena mediated by phonons can trigger an avalanche of electrons which will momentarily fill the energy levels of the TQD, thereby lowering the level of the EQD, which would allow for an electron to fill it by tunneling from the left lead. This would make a jump back to the OFF branch momentarily possible, leading back to the situation in Fig. 1(h)8. The hysteretic nature of this phonon catalysis would allow for these multiple jumps only in the forward path but not during the reverse path. Indeed, according to polaron dynamics^{35,36}, a population inversion between two phononic minima occurring around $V = E_-$ would change the interaction between the electrons and the phonons such that the phonons would favorably be in a higher potential well allowing for the reverse jump during the forward sweep, but they would be in the lower well during the reverse sweep, thus stabilizing the device in the OFF state. We point out that this hysteretic population change of the phonons could be linked to a structural rearrangement of the surroundings of the C atoms, notably in the angles of its bondings with the leads and the other species involved in transport^{34,37}. We also note that, depending on the position of the energy levels of the transport quantum dots relative to the environmental quantum dot, the events E_- or E_+ may or may not occur around a conductance peak. A situation where the jump at E_+ occurs inside the Coulomb blockade region is presented in Fig. 1(d) and in SI Fig.S4. We described the situation of Fig. 1(b), but we can easily convince ourselves that if we place the upper levels of the TQD below the empty level of the EQD in the ON state, the potential of the left electrodes would address the level of the EQD around $V = E_-$ before reaching the edge of the Coulomb blockade region.

The discrete energy levels of the transport and environmental quantum dots give rise to quantum transport interference effects. We present in Fig. 2(a) the temperature dependence of the resistance R measured on junction G10 at $V = -170$ mV. As seen in Fig. 1(c), the junction is bistable at 10 K at this bias. Upon cooling down from 140K, the current broadens into two branches ON and OFF, with intermediate spectral weight of low intensity (MID branch). Further evidence of these regimes appears in SI Note 7. Since temperature alone can promote a dominant transport branch, we conclude that electron-phonon interactions, i.e. vibrons, also be involved in the quantum interference transport here, in line with prior literature^{35,38-40}.

We use bias-dependent current statistics to observe transport branches due to quantum interference. We begin by plotting in Fig. 2(b) differential conductance data in the P magnetic state of junction C5 at $T = 10$ K. On

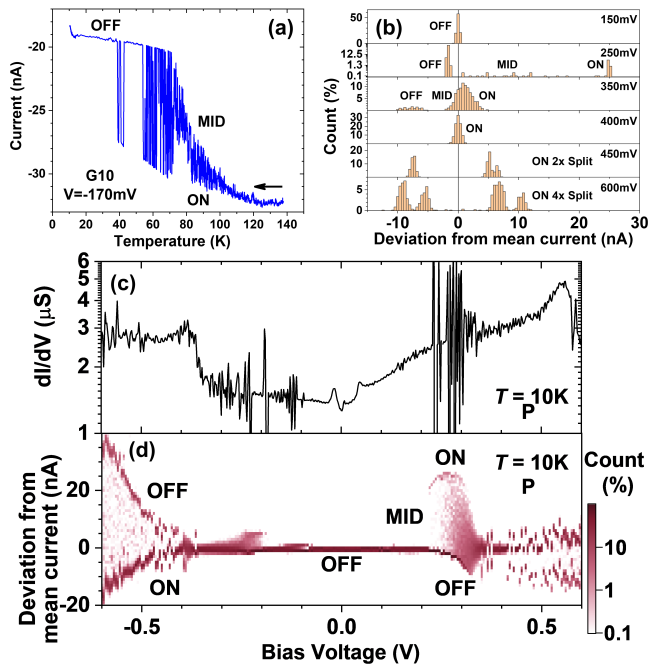


Figure 2. **Quantum transport interference between individual carbon atoms.** (a) Intensity as function of temperature at -2000 Oe and -170 mV. (c) Differential conductance of junction C5 at 10 K for the P magnetic state. (d) Color map of the statistic weight of the current deviation from the mean current as a function of applied bias of junction C5. The junction P magnetic state was used. At each bias value, 1000 current measurements were acquired. Datasets at select voltage values are shown in panel (b).

the log scale, we observe sizeable increases in conductance, and the clear appearance of noise for $V < -0.4$ V and for $V > 0.3$ V. Within $-0.6 < V$ (V) $< +0.6$, after setting the dc applied bias, we measured the current 1000 times. The statistics of a given current deviation from the mean current as a function of applied bias are plotted in panel (c). Within $|V| < 0.2$ V, the current remains essentially stable along the OFF branch. For $|V| > 0.2$ V, the transition to the MID state can appear. This is especially visible within $0.2 < V$ (V) < 0.4 . While the OFF branch shifts to values below the mean, the MID branch collapses into the dominant branch around $V = 0.4$ V. A higher resolution map of this region is shown in SI Note 1. For $V > 0.4$ V, this branch splits into two branches labelled ON and OFF. A similar branching is seen for $V < -0.4$ V. Erratically, each of these two branches can split into two subbranches, for a total of four branches (see Fig. 2(d)). The noise in conductance thus arises from transport interference between these branches which are visualized by our current statistics.

Overall, these experimental findings support a picture of vibron-mediated co-tunnelling and/or Coulomb drag between nanotransport paths² due to blockade effects such as Franck-Condon blockade³⁸. According to the theory of out-of-equilibrium polaron dynamics^{35,36}, trans-

port through an impurity with discrete energy levels such as a quantum dot or a molecular orbital which is strongly coupled to a vibrational degree of freedom and tunnel coupled to two leads explains the observed multi-stability of different states and the telegraphic switching between the different intensity branches. The voltage acts as an effective temperature and a force modulating the potential of the oscillator. Around specific voltage biases, the effective vibron energy potential landscape develops several minima, and thus promotes metastability between different occupation states. Two scenarios are possible. 1) Thermally activated switching between different intensity branches related to each of the well separated potential minima can occur⁷. 2) Large fluctuations around a single intensity branch occur when at least two minima are close enough so that the quasi-degenerate states they encode trigger an interference effect^{41,42}. In this latter case, intermediate states outside the well minima are measured.

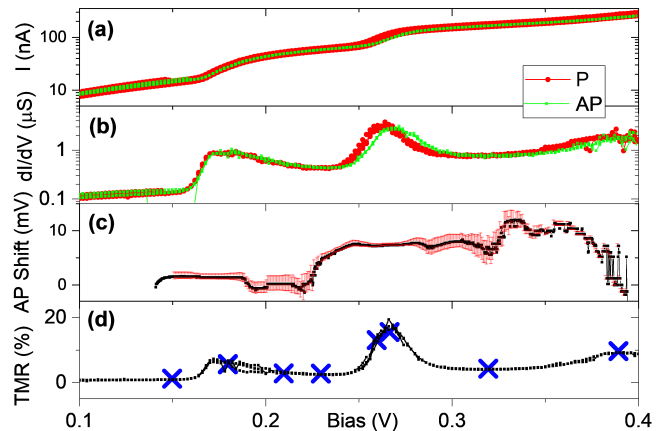


Figure 3. **Spintronic impact of Coulomb blockade along transport branches.** a) Current-voltage characteristic for the P and AP junction states, and (b) the resulting dI/dV differential conductance. (c) Voltage shift between the P and AP conductance data (see Methods for details). (d) Bias dependence of the TMR from calculated from (a). Blue crosses indicate TMR amplitudes obtained from $I(H)$ experiments.

The memristive behavior of the Coulomb blockade peak due to environmental charging represents one level of information encoding. Repeated testing indicates a write success rate of at least 81% (see SI Note 3). The MTJ's two ferromagnetic leads enable us to examine how the spin polarization of the charge current impacts the atom-level memristive Coulomb blockade effect and quantum interference effects. To experimentally obtain spintronic contrast in our data, we examine the impact on transport of switching the orientation of electrode magnetization from parallel (P) to antiparallel (AP). The tunnel magnetoresistance $TMR = \frac{I_P}{I_{AP}-1}$ characterizes to what extent the two spin channels of current flowing across the device are asymmetric. Within the widely used Julliere model⁴³, this asymmetry arises from the spin-polarized densities of states of the ferromagnetic elec-

trodes, and was extended to effectively encompass the filtering of electronic symmetries with majority spin polarization during solid-state tunnelling across MgO^{44,45}.

We plot in Fig. 3(a) the IV in the MTJ's P and AP states at $T = 10$ K. Both exhibit a series of plateaus and increases that are absent in junctions without C atoms^{21–23}. The corresponding differential conductance (dI/dV) data (see panel (b)) reveals a series of peaks. While the P and AP datasets share similar traits, the AP plot appears to shift to higher bias as the onset of each conductance increase is reached. This is confirmed through an analysis of the correlated shift between the two datasets in Fig. 3(c) (see Methods).

In our MgO MTJs without C²¹, we observe TMR $\approx 200\%$ at 10 K around $V = 0$, and a mostly monotonous TMR decreasing with increasing $|V|$. When C atoms are introduced into MgO, we observe only a few % TMR around $V = 0$. Instead, due to the shift in AP conductance to higher bias with each succeeding conductance peak, the TMR bias dependence closely mimics the junction conductance (compare panels (c) and (d) of Fig. 3). This highly structured TMR bias dependence is confirmed through discrete $I(H)$ datasets at fixed V (crosses in Fig. 3(d)). We observe local TMR maxima precisely on the conductance peaks, with an absolute maximum of 15%.

To discuss the impact on spintronics of the memristive Coulomb blockade effect, we present $I(H)$ data in Fig. 1(g) in both the ON and off state of the junction, taken at $V = -50$ mV; i.e. precisely at the bias value corresponding to the memristive Coulomb blockade peak shown in panels (c-e) of Fig. 1. We observe that I_P increases and that $I_{P-I_{AP}}$ is multiplied by 7, so that the TMR increases from 0.5% in the OFF state to 3.7% in the ON state due to the Coulomb blockade peak. Within the paradigm of MgO tunnelling spintronics⁴⁶, this suggests that the Coulomb blockade peak effectively opens an additional transport channel with dominant majority spin carriers.

According to the theoretical work of Płomińska and Weymann⁴⁷, the similar set of bias-dependent conductance peaks in the MTJ's P and AP states, leading to a similar TMR trace, is the signature of a special kind of Coulomb blockade effect named Pauli Spin blockade^{48–50}. As the electronic level of the carbon transport atom is reached with applied bias, sequential tunneling is suppressed while co-tunnelling mechanisms become dominant and modify the spin state (and eventually the charge¹²) of the paramagnetic C atom, as a form of spintronic anisotropy^{51–53}. With increasing voltage, the FeCoB/MgO tunnelling-induced accumulation of mostly spin up carriers lifts degeneracy of the spin states. This effectively lowers the spin up state relative to the spin down state. This spin splitting differs between the MTJ's P and AP states due to different energy alignments of the C electronic levels^{12,47}. This effect is also modeled by our schematic in Fig 1(h) which features this spin splitting. Indeed, we witness that in the P state of the the elec-

trodes presented in this figure, the potential of the electrodes will align with the split spin energy levels of the transport quantum dot at lower absolute bias than in the AP state, which would result in a voltage shift between the onsets of the conductance peaks leading to a positive TMR. SI Notes 1 and 4 provide additional evidence of this effect.

The conductance shift of Fig.3(c) is thus an experimental manifestation of spin accumulation. Spin accumulation also explains the shift in quantum interference data and the spin polarization of the transport branch therein (see SI Note 2). It also explains why the TMR bias dependence tracks that of junction conductance (see Fig. 3(d)), as well as the huge increase in $I_{P-I_{AP}}$ due to the memristive Coulomb peak (see Fig. 1(g)) leading to the seven-fold TMR enhancement. The best agreement between the results of Płomińska and Weymann⁴⁷ and our experimental datasets is that of 'parallel' or 'T-shaped' electronic transport across spin states, rather than the other series scenario proposed. This supports the atomic description of the effective nanotransport path across our microscale MTJs.

To conclude, inserting C atoms into ultrathin MgO layers generates localized paramagnetic¹² states. Experiments on micronic FeCoB/MgO/FeCoB magnetic tunnel junctions, which are crafted using straightforward technological processes, show that the effective nanotransport path²² involves individual C atoms. Their discrete energy levels promote Coulomb blockade effects that can be reproducibly shifted in energy by charging events on neighboring C atoms. The tunnel coupling between these transport and environmental carbon atoms promotes quantum interference effects. Spin-polarized transport induces spin accumulation that lifts the spin degeneracy of the unpaired C electron in MgO. This leads to a voltage shift in Coulomb peaks and quantum interference effects between the datasets in the MTJ's P and AP magnetic states. Spin accumulation also accounts for the huge enhancement of the spintronic performance when a Coulomb peak is memristively controlled. We thus demonstrate how to use both the electron charge and spin to encode information on an individual paramagnetic atom in a solid-state, industrializable device. These results showcase MgO tunnelling spintronics as a promising industrial platform for quantum technologies at potentially practical temperatures, to deploy quantum transport effects that are normally only seen in model junctions. One track to achieve these effects at room temperature will be to engineer the impedances that electronically link the transport and environmental atoms to the magnetic tunnel junction electrodes. Final applications of quantum spintronics not only encompass information encoding¹¹, but also energy harvesting^{12,13} vectors.

Methods Glass//Ta(5)/Co(10)/IrMn(7.5)/CoFeB(4)/MgO(0.9)/C(0.6)MgO(1.7)/CoFeB(3)/Ta(2)/Pt(1) samples (all thicknesses in nm) were sputter-grown on Corning 1737 glass substrates⁵⁴. Stacks were post-annealed in an in-plane magnetic field of 200 Oe for

one hour at a temperature T_a of 200 °C to magnetically pin the lower electrode thanks to the IrMn antiferromagnetic layer. Samples were then processed by optical lithography⁵⁵ into 20 μm -diameter MTJs, and measured on a variable-temperature magnetotransport bench. 54 junctions were tested on these samples, 35 of them were either metallic or open circuit. Among the other 19 interesting junctions, all the reported effects have been observed in several of them. 8 of them presented memristive properties with branch jumps and conductance peaks, among which at least 3 presented magnetomemristive properties correlating with the conductance, while 7 of them presented jumps and noisy behaviors typical of interferences between several nanotransport paths (see SI Note 6).

Acknowledgements We gratefully acknowledge PhD funding for M.L. from Ecole Polytechnique. We acknowledge financial support from the ANR (ANR-21-CE50-0039), the Contrat de Plan Etat-Region grants in 2006 and 2008, by “NanoTérahertz”, a project co-funded by the ERDF 2014–2020 in Alsace (European Union fund) and by the Region Grand Est through its FRCR call, by the impact project LUE-N4S part of the French PIA project “Lorraine Université d’Excellence”, reference ANR-15IDEX-04-LUE and by the FEDER-FSE “Lorraine et Massif Vosges 2014–2020”, a European Union Program. This work of the Interdisciplinary Thematic Institute QMat, as part of the ITI 2021-2028 program of the University of Strasbourg, CNRS and Inserm, was supported by IdEx Unistra (ANR 10 IDEX 0002), and by SFRI STRAT’US project (ANR 20 SFRI 0012) and EUR QMAT ANR-17-EURE-0024 under the framework of the French Investments for the Future Program.

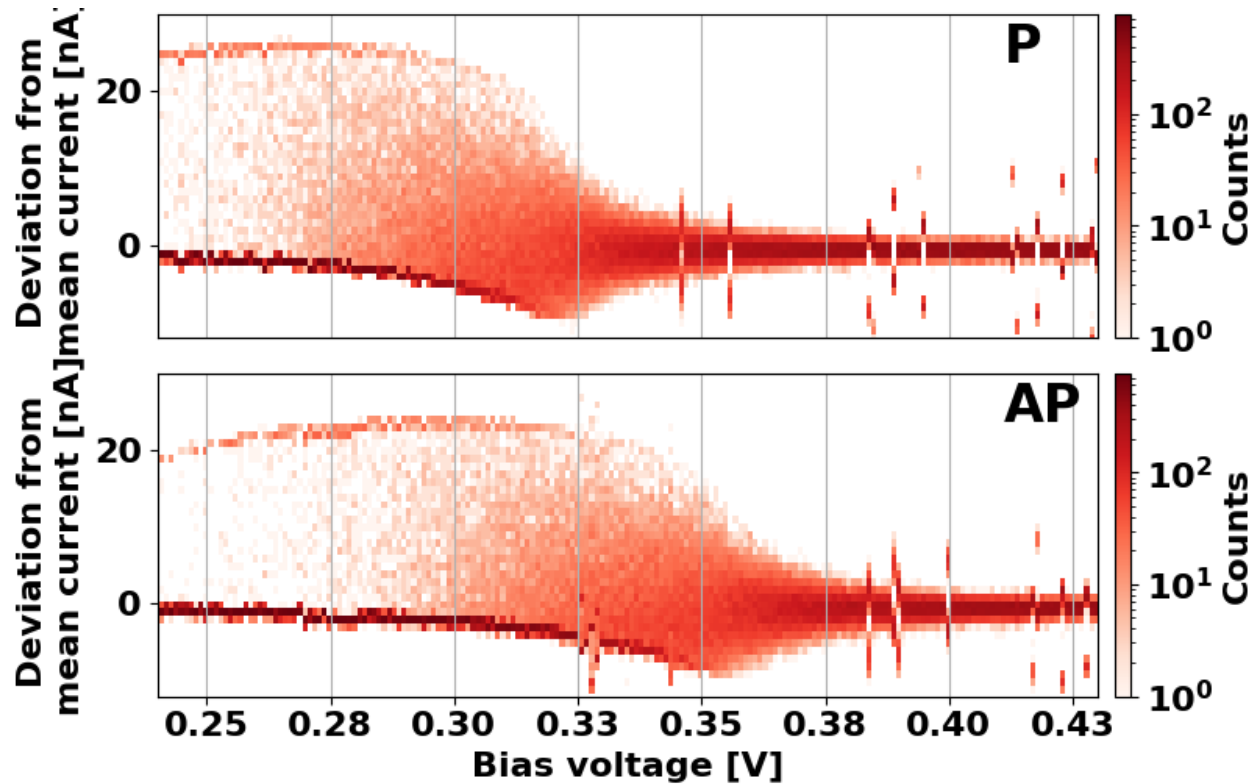
REFERENCES

- ¹D. A. Ryndyk, “Electron-Electron Interaction and Coulomb Blockade,” in *Theory of Quantum Transport at Nanoscale*, Vol. 184 (Springer International Publishing, Cham, 2016) pp. 123–147.
- ²A. Keller, J. Lim, D. Sánchez, R. López, S. Amasha, J. Katine, H. Shtrikman, and D. Goldhaber-Gordon, “Cotunneling Drag Effect in Coulomb-Coupled Quantum Dots,” *Physical Review Letters* **117** (2016), 10.1103/PhysRevLett.117.066602.
- ³E. Burzuri, Y. Yamamoto, M. Warnock, X. Zhong, K. Park, A. Cornia, and H. S. J. van der Zant, “Franck–condon blockade in a single-molecule transistor,” **14**, 3191–3196 (2014).
- ⁴M. Ganzhorn, S. Klyatskaya, M. Ruben, and W. Wernsdorfer, “Strong spin–phonon coupling between a single-molecule magnet and a carbon nanotube nanoelectromechanical system,” **8**, 165–169 (2013).
- ⁵J. J. Parks, A. R. Champagne, T. A. Costi, W. W. Shum, A. N. Pasupathy, E. Neuscamman, S. Flores-Torres, P. S. Cornaglia, A. A. Aligia, C. A. Balseiro, G. K.-L. Chan, H. D. Abruña, and D. C. Ralph, “Mechanical control of spin states in spin-1 molecules and the underscreened kondo effect,” **328**, 1370–1373 (2010).
- ⁶T. Miyamachi, M. Gruber, V. Davesne, M. Bowen, S. Boukari, L. Joly, F. Scheurer, G. Rogez, T. K. Yamada, P. Ohresser, E. Beaurepaire, and W. Wulfhchel, “Robust spin crossover and memristance across a single molecule,” *Nature Communications* **3**, 938 (2012).
- ⁷S. J. van der Molen and P. Liljeroth, “Charge transport through molecular switches,” **22**, 133001 (2010).
- ⁸D. Secker, S. Wagner, S. Ballmann, R. Härtle, M. Thoss, and H. B. Weber, “Resonant Vibrations, Peak Broadening, and Noise in Single Molecule Contacts: The Nature of the First Conductance Peak,” *Physical Review Letters* **106** (2011), 10.1103/PhysRevLett.106.136807.
- ⁹Y.-J. Zeng, D. Wu, X.-H. Cao, Y.-X. Feng, L.-M. Tang, and K.-Q. Chen, “Significantly enhanced thermoelectric performance of molecular junctions by the twist angle dependent phonon interference effect,” **8**, 11884–11891 (2020).
- ¹⁰J. E. Greenwald, J. Cameron, N. J. Findlay, T. Fu, S. Gunasekaran, P. J. Skabara, and L. Venkataraman, “Highly nonlinear transport across single-molecule junctions via destructive quantum interference,” **16**, 313–317 (2020).
- ¹¹K. Katcko, E. Urbain, F. Ngassam, L. Kandpal, B. Chowrira, F. Schleicher, U. Halisdemir, D. Wang, T. Scherer, D. Mertz, B. Leconte, N. Beyer, D. Spor, P. Panissod, A. Boulard, J. Arabski, C. Kieber, E. Sternitzky, V. Da Costa, M. Hehn, F. Montaigne, A. Bahouka, W. Weber, E. Beaurepaire, C. Kübel, D. Lacour, M. Alouani, S. Boukari, and M. Bowen, “Encoding Information on the Excited State of a Molecular Spin Chain,” *Advanced Functional Materials* **31**, 2009467 (2021).
- ¹²K. Katcko, E. Urbain, B. Taudul, F. Schleicher, J. Arabski, E. Beaurepaire, B. Vilenó, D. Spor, W. Weber, D. Lacour, S. Boukari, M. Hehn, M. Alouani, J. Fransson, and M. Bowen, “Spin-driven electrical power generation at room temperature,” *Communications Physics* **2** (2019), 10.1038/s42005-019-0207-8.
- ¹³B. Chowrira, L. Kandpal, D. Mertz, C. Kieber, A. Bahouka, R. Bernard, L. Joly, E. Monteblanco, S. Mohapatra, H. P. Garcia, S. Elidrissi, M. Gavara, E. Sternitzky, V. D. Costa, M. Hehn, F. Montaigne, B. Vilenó, F. Choueikani, P. Ohresser, D. Lacour, W. Weber, S. Boukari, and M. Bowen, “need to update,” (2020), arXiv:2009.10413 [cond-mat.mes-hall].
- ¹⁴C. Barraud, K. Bouzehouane, C. Deranlot, D. J. Kim, R. Rakshit, S. Shi, J. Arabski, M. Bowen, E. Beaurepaire, S. Boukari, F. Petroff, P. Seneor, and R. Mattana, “Phthalocyanine based molecular spintronic devices,” *Dalton Transactions* **45**, 16694–16699 (2016).
- ¹⁵M. Bowen, J.-L. Maurice, A. Barthélémy, P. Prod’homme, E. Jacquet, J.-P. Contour, D. Imhoff, and C. Colliex, “Bias-crafted magnetic tunnel junctions with bistable spin-dependent states,” *Applied Physics Letters* **89**, 103517 (2006).
- ¹⁶A. D. Kent and D. C. Worledge, “A new spin on magnetic memories,” *Nature Nanotechnology* **10**, 187–191 (2015).
- ¹⁷J. Torrejon, M. Riou, F. A. Araujo, S. Tsunegi, G. Khalsa, D. Querlioz, P. Bortolotti, V. Cros, K. Yakushiji, A. Fukushima, H. Kubota, S. Yuasa, M. D. Stiles, and J. Grollier, “Neuromorphic computing with nanoscale spintronic oscillators,” *Nature* **547**, 428–431 (2017).
- ¹⁸L. Zhang, B. Fang, J. Cai, M. Carpentieri, V. Puliafitto, F. Garesci, P. K. Amiri, G. Finocchio, and Z. Zeng, “Ultrahigh detection sensitivity exceeding 10^5 V/W in spin-torque diode,” *Applied Physics Letters* **113**, 102401 (2018).
- ¹⁹P. P. Freitas, R. Ferreira, S. Cardoso, and F. Cardoso, “Magnetoresistive sensors,” *Journal of Physics-Condensed Matter* **19** (2007), 10.1088/0953-8984/19/16/165221.
- ²⁰Y. Lu, M. Tran, H. Jaffrès, P. Seneor, C. Deranlot, F. Petroff, J.-M. George, B. Lépine, S. Ababou, and G. Jézéquel, “Spin-Polarized Inelastic Tunneling through Insulating Barriers,” *Physical Review Letters* **102**, 176801 (2009).
- ²¹F. Schleicher, U. Halisdemir, D. Lacour, M. Gallart, S. Boukari, G. Schmerber, V. Davesne, P. Panissod, D. Halley, H. Majjad, Y. Henry, B. Leconte, A. Boulard, D. Spor, N. Beyer, C. Kieber, E. Sternitzky, O. Cregut, M. Ziegler, F. Montaigne, E. Beaurepaire, P. Gilliot, M. Hehn, and M. Bowen, “Localized states in advanced dielectrics from the vantage of spin- and symmetry-polarized tunnelling across MgO,” *Nature Communications* **5** (2014), 10.1038/ncomms5547.
- ²²M. Studniarek, U. Halisdemir, F. Schleicher, B. Taudul, E. Ur-

- bain, S. Boukari, M. Hervé, C.-H. Lambert, A. Hamadeh, S. Petit-Watelot, O. Zill, D. Lacour, L. Joly, F. Scheurer, G. Schmerber, V. D. Costa, A. Dixit, P. A. Guitard, M. Acosta, F. Leduc, F. Choueikani, E. Otero, W. Wulfhchel, F. Montaigne, E. N. Montebancho, J. Arabski, P. Ohresser, E. Beaurepaire, W. Weber, M. Alouani, M. Hehn, and M. Bowen, "Probing a device's active atoms," *Advanced Materials* **29**, 1606578 (2017).
- ²³F. Schleicher, B. Taudul, U. Halisdemir, K. Katcko, E. Montebancho, D. Lacour, S. Boukari, F. Montaigne, E. Urbain, L. M. Kandpal, J. Arabski, W. Weber, E. Beaurepaire, M. Hehn, M. Alouani, and M. Bowen, "Consolidated picture of tunnelling spintronics across oxygen vacancy states in MgO," *Journal of Physics D: Applied Physics* **52**, 305302 (2019).
- ²⁴B. Taudul, E. N. Montebancho, U. Halisdemir, D. Lacour, F. Schleicher, F. Montaigne, E. Beaurepaire, S. Boukari, M. Hehn, M. Alouani, and M. Bowen, "Tunneling Spintronics across MgO Driven by Double Oxygen Vacancies," *Advanced Electronic Materials* **3**, 1600390 (2017).
- ²⁵E. Bertin, D. Halley, Y. Henry, N. Najjari, H. Majjad, M. Bowen, V. DaCosta, J. Arabski, and B. Doudin, "Random barrier double-well model for resistive switching in tunnel barriers," *Journal of Applied Physics* **109**, 083712 (2011).
- ²⁶J. M. Aguiar-Hualde and M. Alouani, "Taming the resistive switching in Fe/MgO/V/Fe magnetic tunnel junctions: An ab initio study," *Journal of Magnetism and Magnetic Materials* **372**, 167–172 (2014).
- ²⁷I. Hwang, M.-J. Lee, G.-H. Buh, J. Bae, J. Choi, J.-S. Kim, S. Hong, Y. S. Kim, I.-S. Byun, S.-W. Lee, S.-E. Ahn, B. S. Kang, S.-O. Kang, and B. H. Park, "Resistive switching transition induced by a voltage pulse in a Pt/NiO/Pt structure," *Applied Physics Letters* **97**, 052106 (2010).
- ²⁸C. Jia, A. Migliore, N. Xin, S. Huang, J. Wang, Q. Yang, S. Wang, H. Chen, D. Wang, B. Feng, Z. Liu, G. Zhang, D.-H. Qu, H. Tian, M. A. Ratner, H. Q. Xu, A. Nitzan, and X. Guo, "Covalently bonded single-molecule junctions with stable and reversible photoswitched conductivity," *Science* **352**, 1443–1445 (2016).
- ²⁹E. Lörtcher, J. Ciszek, J. Tour, and H. Riel, "Reversible and controllable switching of a single-molecule junction," **2**, 973–977 (2006).
- ³⁰F. Schwarz, G. Kastlunger, F. Lissel, C. Egler-Lucas, S. N. Semenov, K. Venkatesan, H. Berke, R. Stadler, and E. Lörtcher, "Field-induced conductance switching by charge-state alternation in organometallic single-molecule junctions," *Nature Nanotechnology* **11**, 170–176 (2016).
- ³¹S. W. Wu, N. Ogawa, G. V. Nazin, and W. Ho, "Conductance Hysteresis and Switching in a Single-Molecule Junction," *The Journal of Physical Chemistry C* **112**, 5241–5244 (2008).
- ³²T. Leoni, O. Guillermet, H. Walch, V. Langlais, A. Scheuermann, J. Bonvoisin, and S. Gauthier, "Controlling the Charge State of a Single Redox Molecular Switch," *Physical Review Letters* **106** (2011), 10.1103/PhysRevLett.106.216103.
- ³³L. Gerhard, K. Edelmann, J. Homberg, M. Valášek, S. G. Baehoosh, M. Lukas, F. Pauly, M. Mayor, and W. Wulfhchel, "An electrically actuated molecular toggle switch," *Nature Communications* **8**, 14672 (2017).
- ³⁴L. Zhang, T. Yang, W. Zhang, D. Qi, X. He, K. Xing, P. K. J. Wong, Y. P. Feng, and A. T. S. Wee, "Bi-stable electronic states of cobalt phthalocyanine molecules on two-dimensional vanadium diselenide," *Applied Materials Today* **18**, 100535 (2020).
- ³⁵D. Mozyrsky, M. B. Hastings, and I. Martin, "Intermittent polaron dynamics: Born-Oppenheimer approximation out of equilibrium," *Physical Review B* **73** (2006), 10.1103/PhysRevB.73.035104.
- ³⁶M. Galperin, M. A. Ratner, and A. Nitzan, "Hysteresis, Switching, and Negative Differential Resistance in Molecular Junctions: A Polaron Model," *Nano Letters* **5**, 125–130 (2005).
- ³⁷J. Martínez-Blanco, C. Nacci, S. C. Erwin, K. Kanisawa, E. Locane, M. Thomas, F. von Oppen, P. W. Brouwer, and S. Fölsch, "Gating a single-molecule transistor with individual atoms," *Nature Physics* **11**, 640–644 (2015).
- ³⁸J. Koch, F. von Oppen, and A. V. Andreev, "Theory of the Franck-Condon blockade regime," *Physical Review B* **74** (2006), 10.1103/PhysRevB.74.205438.
- ³⁹M. Galperin, M. A. Ratner, and A. Nitzan, "Molecular transport junctions: vibrational effects," *Journal of Physics: Condensed Matter* **19**, 103201 (2007).
- ⁴⁰S. V. Aradhya and L. Venkataraman, "Single-molecule junctions beyond electronic transport," *Nature Nanotechnology* **8**, 399–410 (2013).
- ⁴¹M. Wierzbicki and R. Swirkowicz, "Influence of interference effects on thermoelectric properties of double quantum dots," *Physical Review B* **84** (2011), 10.1103/PhysRevB.84.075410.
- ⁴²S. W. Wu, G. V. Nazin, X. Chen, X. H. Qiu, and W. Ho, "Control of Relative Tunneling Rates in Single Molecule Bipolar Electron Transport," *Physical Review Letters* **93** (2004), 10.1103/PhysRevLett.93.236802.
- ⁴³M. Julliere, "Tunneling between ferromagnetic films," *Physics Letters A* **54**, 225–226 (1975).
- ⁴⁴M. Bowen, V. Cros, F. Petroff, A. Fert, C. Martinez Boubeta, J. L. Costa-Krämer, J. V. Anguita, A. Cebollada, F. Briones, J. M. de Teresa, L. Morellón, M. R. Ibarra, F. Güell, F. Peiró, and A. Cornet, "Large magnetoresistance in Fe/MgO/FeCo(001) epitaxial tunnel junctions on GaAs(001)," *Applied Physics Letters* **79**, 1655–1657 (2001).
- ⁴⁵V. Kozub, Y. Galperin, and V. Vinokur, "Coulomb blockade-tuned indirect exchange in ferromagnetic nanostructures," *Journal of Magnetism and Magnetic Materials* **465**, 304–308 (2018).
- ⁴⁶J. S. Moodera, G.-X. Miao, and T. S. Santos, "Frontiers in spin-polarized tunneling," *Physics Today* **63**, 46–51 (2010).
- ⁴⁷A. Płomińska and I. Weymann, "Magnetoresistive properties of a double magnetic molecule spin valve in different geometrical arrangements," *Journal of Magnetism and Magnetic Materials* **480**, 11–21 (2019).
- ⁴⁸J. Fransson and M. Räsander, "Pauli spin blockade in weakly coupled double quantum dots," *Physical Review B* **73** (2006), 10.1103/PhysRevB.73.205333.
- ⁴⁹D. M.-T. Kuo, S.-Y. Shiau, and Y.-c. Chang, "Theory of spin blockade, charge ratchet effect, and thermoelectrical behavior in serially coupled quantum dot system," *Physical Review B* **84** (2011), 10.1103/PhysRevB.84.245303.
- ⁵⁰A. Płomińska and I. Weymann, "Pauli spin blockade in double molecular magnets," *Physical Review B* **94** (2016), 10.1103/PhysRevB.94.035422.
- ⁵¹M. Misiorny, I. Weymann, and J. Barnaś, "Spin effects in transport through single-molecule magnets in the sequential and cotunneling regimes," *Physical Review B* **79**, 224420 (2009).
- ⁵²M. Misiorny and I. Weymann, "Transverse anisotropy effects on spin-resolved transport through large-spin molecules," *Physical Review B* **90** (2014), 10.1103/PhysRevB.90.235409.
- ⁵³T. Saygun, J. Bylin, H. Hammar, and J. Fransson, "Voltage-Induced Switching Dynamics of a Coupled Spin Pair in a Molecular Junction," *Nano Letters* **16**, 2824–2829 (2016).
- ⁵⁴J. Bernos, M. Hehn, F. Montaigne, C. Tiusan, D. Lacour, M. Alnot, B. Negulescu, G. Lengaigne, E. Snoeck, and F. G. Aliev, "Impact of electron-electron interactions induced by disorder at interfaces on spin-dependent tunneling in Co-Fe-B/MgO/Co-Fe-B magnetic tunnel junctions," *Physical Review B* **82** (2010), 10.1103/PhysRevB.82.060405.
- ⁵⁵D. Halley, H. Majjad, M. Bowen, N. Najjari, Y. Henry, C. Ulhaq-Bouillet, W. Weber, G. Bertoni, J. Verbeeck, and G. Van Tendeloo, "Electrical switching in Fe/Cr/MgO/Fe magnetic tunnel junctions," *Applied Physics Letters* **92**, 212115 (2008).

Supplementary Information

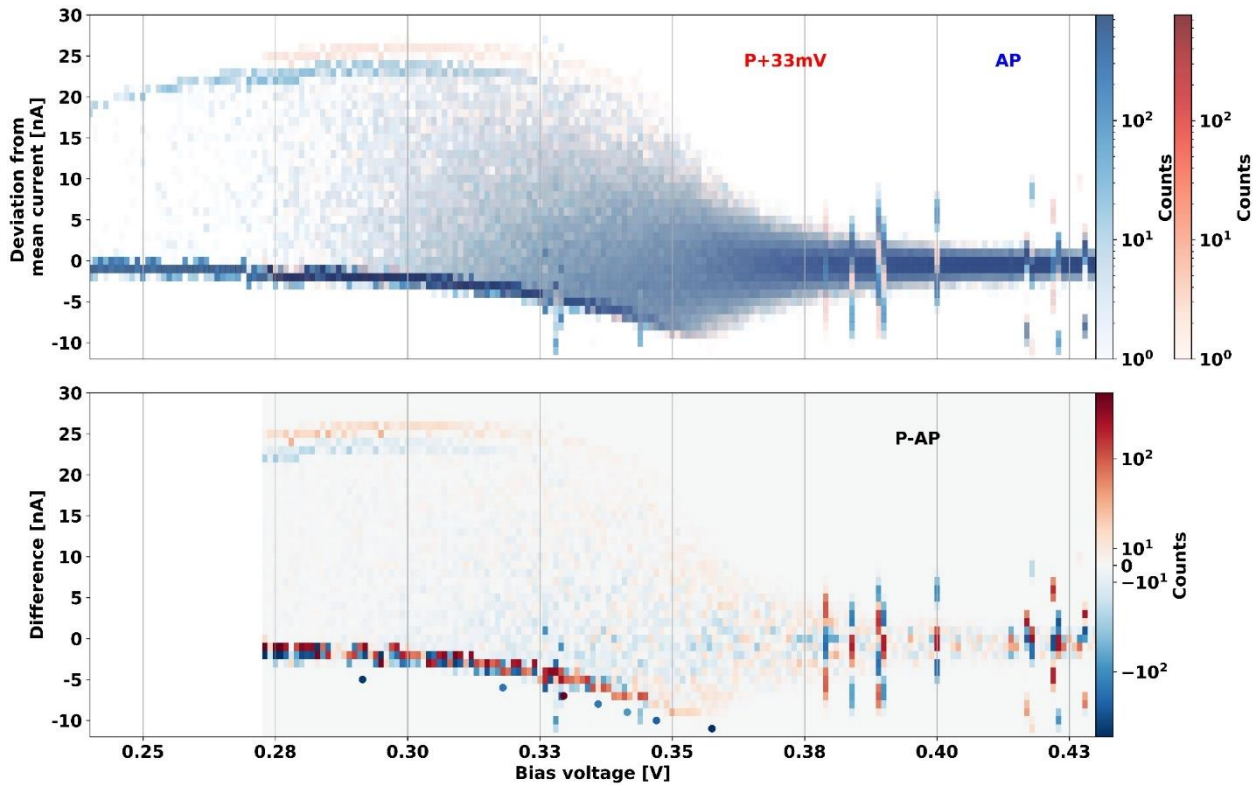
Note 1: Current plume of quantum interference



Suppl. Fig. S1: Zoom on the plume of quantum interference. Bias dependence of the frequency of the deviation from the mean current. Data at $T = 10\text{K}$ in the MTJ's P (top) and AP (bottom) states is shown. Nanojunction C5 was used. Statistics are obtained on 800 points at each bias value.

We present in Suppl . Fig. S1 a high resolution dataset of the current distribution plume reported in Fig. 3 of the main text for the junction's P and AP states. We observe a positive 33mV bias shift of the AP dataset due to spin accumulation (see main text).

For each bias voltage we measured 800 times the junction current. The mean current is calculated and subtracted for all points inside the dataset, and finally an histogram is computed with a bin size of 1nA. The result of the histogram is represented on the Suppl . Fig. S1 by a vertical line of dots at the corresponding voltage bias, the color of a dot representing the number of counts in every bins of the histogram.

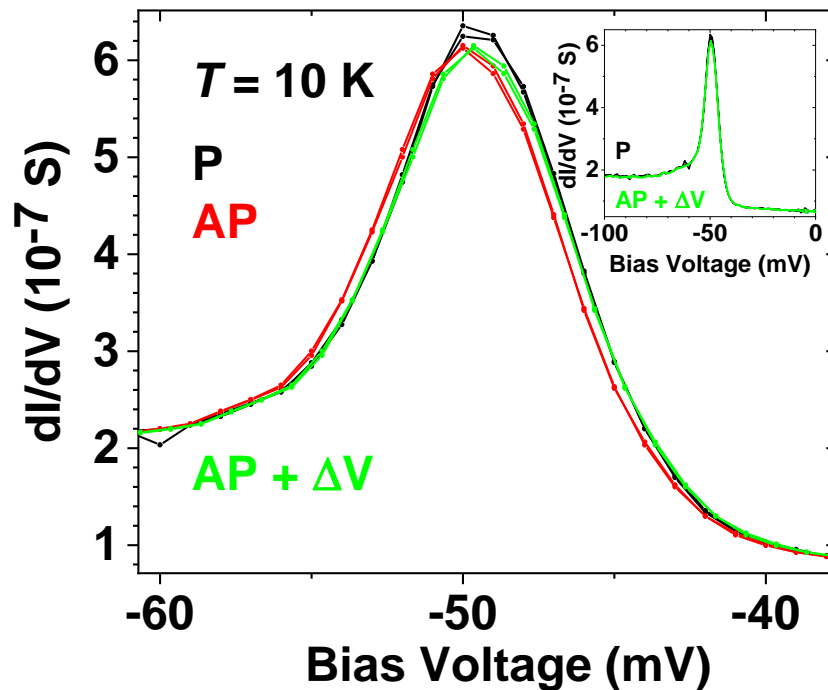


Suppl. Fig. S2: **Spintronic contrast in the plume of quantum interference.** (Top) Same data as in Suppl. Fig S. 1, but with a +33mV shift in the P data. (Bottom) Difference P-AP of the datasets of the top panel. The round dots below the lower branch represent an average of the lower branch difference data. They are centered around the range considered. These points are all blue-leaning: the lower branch is more strongly weighed in the MTJ's AP state.

To distinguish spintronic contrast, we overlap the datasets by manually removing the shift (see Fig. S2a). We note that the OFF branch (lower branch) overlaps rather well. On the other hand, the ON branch (upper branch) exhibits a different deviation from mean current in the MTJ's P and AP states. We attribute this differing deviation to a slight change in the effective potential landscape due to spin-polarized hybridization between the electrodes and the localized paramagnetic barrier states.

To further examine spintronic contrast, we then consider the difference P-AP between the datasets. The results are plotted in the bottom panel of Suppl. Fig. S2. We observe that the difference is very pronounced for the OFF branch. To confirm this trend, we've integrated this difference over several bias ranges. The position of the resulting round dots below the OFF branch represents the center of the range, while the color code shows the averaged result. Over the seven bias ranges considered, all averages of the OFF branch reveal that the OFF branch is more prevalent in the MTJ's AP state. We infer that the transport path responsible for the OFF branch is spin-polarized.

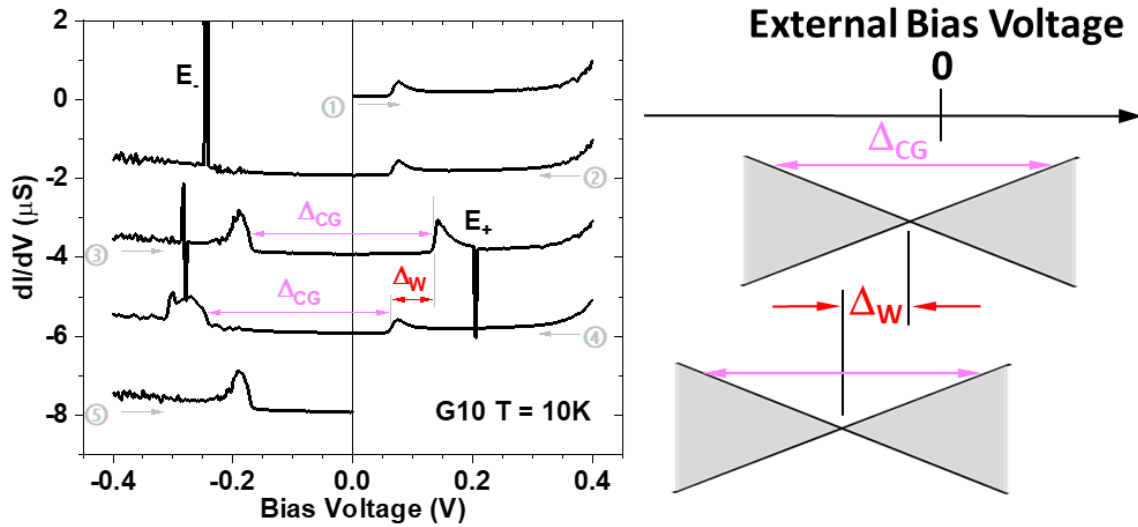
Note 2: Spin accumulation at negative bias



Suppl. Fig. S3: **Spin accumulation on the sharpest Coulomb blockade peak found at $V < 0$.** Bias dependence of differential conductance dI/dV at $T = 10$ K on junction G10 in the MTJ's P (black) and AP (red) states. The AP data in green was bias-shifted by $+0.35$ mV. This shift enables a qualitatively good overlap of the conductance peak with that seen in the P data. Inset: Overview of the conductance peak in the MTJ's P state, and the bias-shifted AP data.

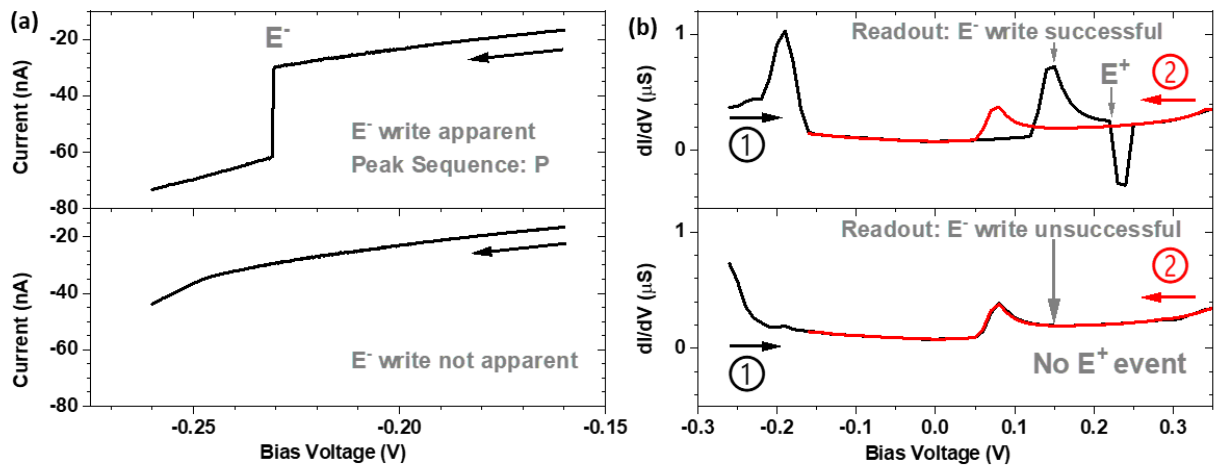
In the main text, we present evidence at $V > 0$ of a shift to higher bias values of the Coulomb blockade peaks when the MTJ's magnetic state is switched from P to AP. We now consider the case of $V < 0$, and focus on the Coulomb blockade peak shown in Suppl. Fig. S3. Its presence can also be switched on/off thanks to writing events $E+$ and $E-$, leading to different values of TMR at that bias position (see Fig. 2 of the main text). The data of Suppl. Fig. S3 is acquired within $-100 < V$ (mV) < 0 , i.e. below the writing events $E-$ and $E+$ (see inset). An excellent overlap between the P and AP data is seen for bias value below the peak. However, as the peak onset is reached, a bias shift is clearly seen. The very close agreement in the data for the forward and reverse scans underscores that the shift is not the result of trivial charging/heating effects. To qualitatively estimate the small bias shift between the P and AP data, we manually shift the AP data. A reasonable fit is found for a bias shift of 0.35 mV.

Note 3: Statistics on the memristive effect



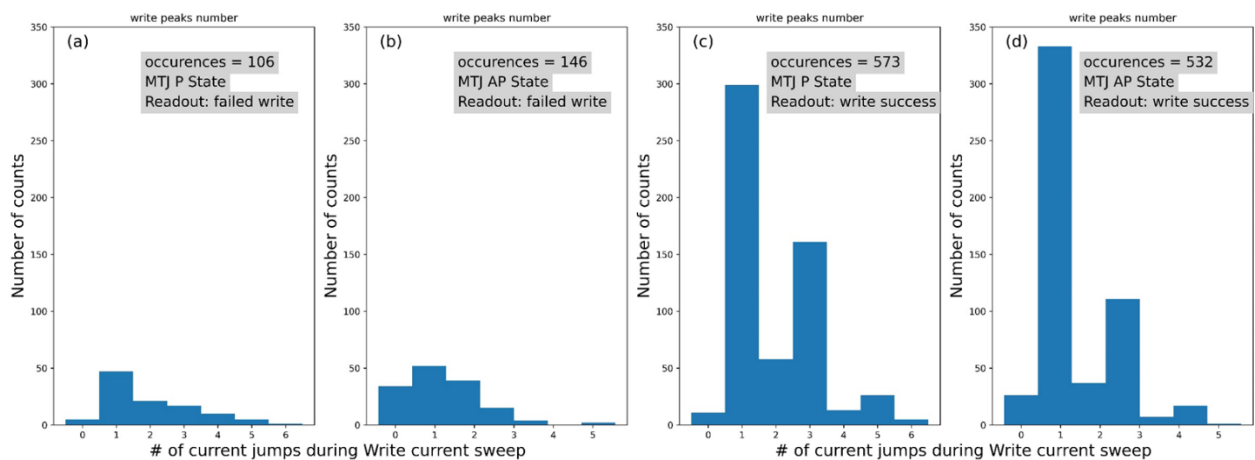
Suppl. Fig. S4: **Overview of the memristive Coulomb diamond shift.** (left) Differential conductance dI/dV vs. bias voltage on junction G10 at 10K. Successive data branches are shifted by $2\mu\text{S}$. The $E+$ and $E-$ writing events cause a shift $\Delta_W=73\text{mV}$ in the constant Coulomb gap $\Delta_{CG}=310\text{mV}$. (Right) Proposed energy diagram of the readout QD in the two $E-$ and $E+$ states. The justification is provided in the discussion to Suppl. Fig. S8.

In the main text, we discuss how current jumps can displace the bias position of pairs of peaks associated with the Coulomb blockade diamond. In this note, we consider the statistics of this electric field-induced shift in the Coulomb diamond. To do so, we first plot an overview of the memristive Coulomb blockade effect in Suppl. Fig. S4. We observe that successive forward and reverse branches reveal a set of two conductance peaks separated by the same $\Delta_{CG} = 310\text{mV}$. The $E+$ and $E-$ writing events cause a shift $\Delta_W=73\text{mV}$ in this pair of conductance peaks.



Suppl. Fig. S5: Protocol to test junction state writing. (a) Examples of IV traces showing E⁻ write events that are (top) apparent, with 1 write peak observed, and (bottom) not apparent, i.e. with no write peak observed. (b) Corresponding readouts, with (top) confirmation and (bottom) information that the E⁻ event-driven junction state was written.

To obtain statistical data on the ability to write a junction state, we undertook 1357 measurements on junction C5 at 10K. Examples of the write and read protocols are shown in Fig. S.5. In general, attempting to activate the E⁻ write event at negative bias generates a 81% success rate in the readout at positive bias. As we explain later, this success rate would likely increase if the maximum voltage of the writing IV protocol had been increased.



Suppl. Fig. S6: Statistics on the success and failure to write the junction state. The repeated protocol shown in SI Fig. S5 was used. The statistics are shown as a function of the number of current jumps during the Write current sweep.

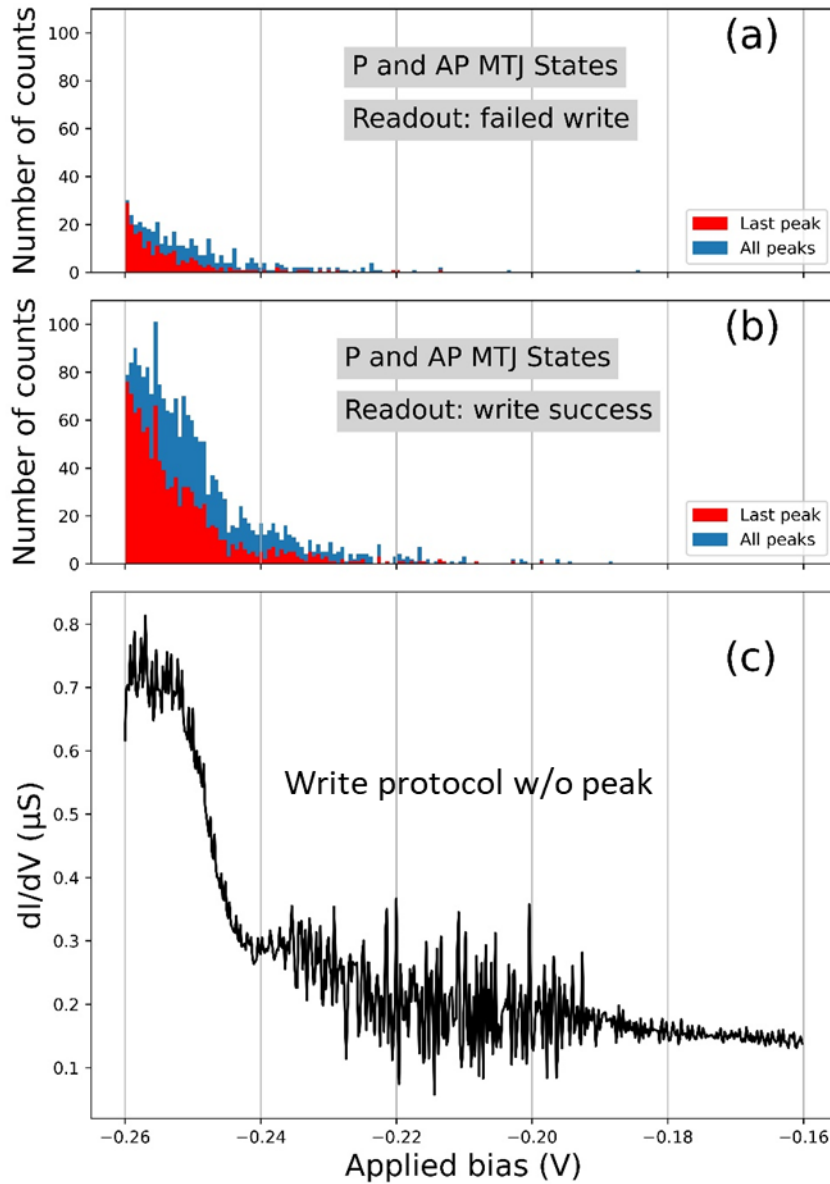
Referring to Suppl. Fig. S6, we note that the failure to write event E- in the MTJ's P state occurs mostly for one current jump, whereas it is spread over 0-2 jumps for the AP state. There are many AP write attempts without a current jump. Furthermore, for both P and AP MTJ states, cases with an odd number of current jumps dominate even cases.

Current Jump sequence (1st ... Last)	Write Failed: # events	Write OK: # events	Write Success (%)
PN	57	93	62
PNPN	14	20	59
PNPNPN	2	2	50
P	88	548	86
PNP	32	271	89
PNPNP	5	43	90
PNPNPNP	1	4	80
No jump	39	37	49

Suppl. Table S1: Statistics of write success/failure according to the sequence of absolute current increase (P) and decrease (N).

To obtain more insight, we examine the sign of current change and current peak sequences in the entire dataset. We observe that:

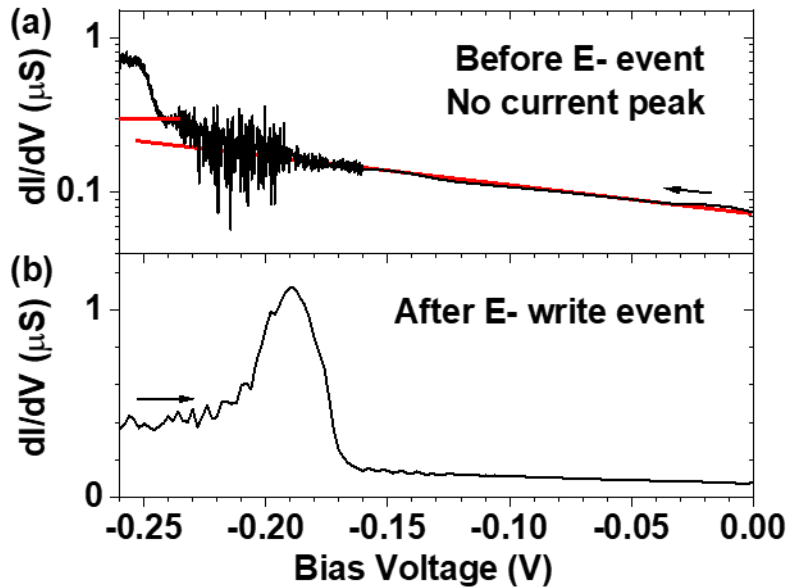
- if there is a peak, the first peak is always P. This means that the first current jump is always to more negative current values.
- the sign of succeeding current peaks is always opposite, i.e. there isn't a single PP or NN sequence or subsequence in our entire dataset.
- an odd number of current jumps (i.e. ending in P) has an overall success rate of 87%. This decreases to 61% for an even number of jumps (i.e. ending in N).



Suppl. Fig. S7 : Spectroscopy of current jumps. Bias dependence of the frequency of a current jump when the writing event (a) fails and (b) succeeds. (c) Bias dependence of junction conductance when no current jump was observed. The average of 60 AP datasets is shown.

We compare in Suppl. Fig. S7 the bias dependencies of the baseline dI/dV for the junction's $E+$ state (i.e. without a current jump / conductance peak), and of the current jump event frequency. We observe that

almost all current jump events occur within the bias range at which a clear conductance increase is observed. We note that the successful write events mimic most closely this dependence/amplitude, while the failed current increase events occur mainly near the peak height. Conversely, very few current jumps, whether successful or not in promoting the E- writing event, are found within the $-0.242 < \text{Bias (V)} < -0.188$ range that exhibits transport noise. We conclude that, for this junction state, the E- writing event begins with the charging of the transport quantum dot, and not with a charging of the environmental quantum dot.



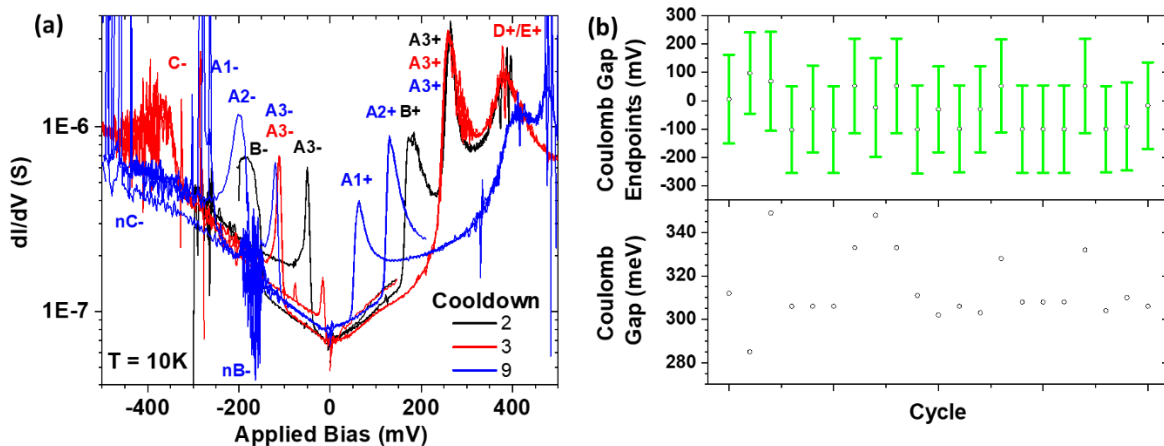
Suppl. Fig. S8: **Origin of transport noise prior to E- event.** (a) dI/dV traces in $E+$ state prior to E- event. Data with no current peak was chosen. The use of the log scale removes negative jumps. The average of 60 scans in the AP MTJ state were used. (b) dI/dV in $E-$ state. Arrows indicate the direction of data acquisition.

We plot in Suppl. Fig. S8(a) dI/dV traces before the E- event, for which no current peak occurs. We observe an exponential increase in junction conductance starting from $V=0$, up to the onset of the very noisy $-0.242 < \text{Bias (V)} < -0.188$ range (red line). Assuming that the conductance exponential increase were to remain the same across this noise range, we see that the conductance at $V = 0.242$ V would be half that measured (straight red line). We conclude that, in this particular junction state, the quantum interference transport between the readout quantum dot and the environmental quantum dot generates a net increase in current, i.e. that the environmental QD participates in transport through higher-order processes.

To verify that readout and environmental QDs with a fortuitously same Coulomb gap (see Suppl. Fig. S4(a)) are not simply trading roles in the E- and E+ events, we plot in panel (b) the dI/dV trace after a successful E- write event. We see that this trace's conductance peak does not have a bias range that matches that for the noise seen in panel (a). Furthermore, the two spectral features do not have the

same bias extent. This suggests that the E- and E+ events do not promote different readout QDs, but that the same QD remains as readout, but with an energy landscape that is shifted by the charging of the environmental QD (see Suppl. Fig. S4(b)). The bias extent and noise envelope of this environmental QD resembles the conductance peak of QD B, but with a +35meV energy shift.

Note 4: Overview of the several Coulomb gaps with evolving junction state and argumentation for single-atom ‘transport’ and ‘environmental’ quantum dots



Suppl. Fig. S9: Overview of Coulomb gap energies with evolving junction state. (a) Select dI/dV traces for three cooldowns. (b) (top) Endpoints of the Coulomb gap for select datasets deduced from the bias spacing of pairs of conductance peaks. (bottom) The resulting Coulomb energy gap of the transport atom. Junction G10 was used. The data from four cooldowns was used.

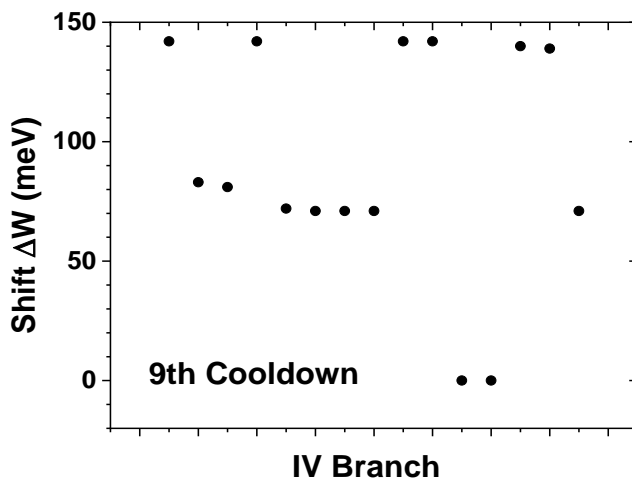
In our datasets, we observe that heating/cooling our FeCoB/MgO/C/MgO/FeCoB junctions, and bias cycling, can alter the effective potential landscape inferred at $T=10K$ from the current derivative. To illustrate these effects, we focus on junction G10. We plot in Suppl. Fig. S9(a) select dI/dV traces obtained after three cooldowns. We have looked for a pattern of pairs of peaks with the same energy spacing as thermal and electrical cycling were conducted. This led us to label pairs of peaks and ascribe them to the charging of a given C atom. In total we identify at least 3, and as many as 5, atoms involved in the device’s electrical response. As described in the main text, these atoms can be in the main transport path. In that case, charging the atom generates a conduction peak. Alternately, the atom in question can be tunnel coupled to a C atom that is in the transport path, and thus constitutes an ‘environmental’ atom. Following the deductions of Suppl. Fig. S9 and accompanying text, we assumed that energy motion of a pair of peaks was due to changes in the environmental charge felt by the transport atom, rather than the reattribution of ‘transport’ and ‘environmental’ roles. This logic is supported by the fairly stable energy gap between the paired peaks (see Suppl. Fig. S9(b)).

Using this labelling logic, we find for example, for cooldown #9, that pairs of conductance peaks can be attributed to the same carbon atom A, and that, in the course of IV cycling, three absolute energy positions of its Coulomb gap (see labels A1-, A2-, A3- and A1+, A2+ and A3+ in Suppl. Fig. S9(a)) relative to the MTJ electrodes' Fermi level can be tracked as the environmental charge is varied through write events E+ and E- (see main Text). Note how after an E+ writing event the pair of peaks shifts to lower absolute bias. The reverse occurs for an E- writing event. This trend in the bias shift was systematically observed, when a shift indeed occurred (see SI Note 2).

We observe additional conductance peaks at higher absolute bias voltage. In the absence of a clear trend suggesting additional charging of atom A, we surmise that these peaks correspond to additional atoms (C, D...) directly in the transport path.

Comparing these cooldowns, we observe that the peak of a dI/dV in one cooldown can spectrally correspond to noise for another cooldown. The best example is, at $V \sim -190\text{mV}$, that of peak B- in cooldown 2 (black), and of the corresponding noise nB- in cooldown 9 (blue). We infer that atom B is present in the transport path in cooldown 2, but becomes an environmental atom in cooldown 9. This also explains the absence of peaks B- and B+ in cooldowns 3 and 9.

We also observe that, in the junction state defined by cooldowns 3 and 9, the writing event E+ occurs just as the spectral window B+ corresponding to environmental atom B is reached with increasing positive bias around +150 mV. This illustrates the role that the charge state of environmental atom has in the junction write process (see main text).



Suppl. Fig. S10: Quantization of the energy shift of the transport atom's Coulomb gap. Absolute values are shown.

Within the junction state defined by a cooldown, writing events E- and E+ generate an effective bias shift that can be quantized. A $\sim 75\text{meV}$ shift was observed on transport atom A during the 1357 tests of the E- and E+ event after cooldown 10 (see SI Note 2). A shift of 111meV was observed on atom B in a

transport role, However, those junction states promoted only two pairs of peaks. We present in Suppl. Fig. S10 the energy shift ΔW data in junction cooldown 9 arising from the presence of 3 pairs of peaks due to transport atom A. Aside from the trivial $\Delta W=0$ points due to write failure (see SI Note 2), DW takes on multiple values of 70-80meV. Here, we make the reasonable assumption that the charge of an environmental atom can only change by 1 electron, which implies that several environmental atoms can be charged during a write event.

Note 5: Estimation of the impurities sizes and distances

Let us approximate the impurity involved in transport as a sphere of radius r , located at a distance d from the lower electrode, with interelectrode spacing l . In the far-field limit, the capacitance C is given in Ref. 1 and reads:

$$C = \frac{4\pi\epsilon\epsilon_0 r}{1 + \left(\psi^{(0)}\left(\frac{d}{l}\right) + \psi^{(0)}\left(1 - \frac{d}{l}\right) + 2\gamma\right) \frac{r}{2l}},$$

where $\psi^{(0)}$ is the polygamma function. Using the relation between the capacitance and the charging energy $E_C = e^2/2C = e\Delta_{CG}$, we obtain the radius of the impurity

$$r = \frac{l}{8\pi\epsilon\epsilon_0 \Delta_{CG}/e + 5/3}$$

where $\frac{1}{2}(\psi^{(0)}(d/l) + \psi^{(0)}(1 - d/l) + 2\gamma) \approx -5/3$ with $d = 1$ nm and $l = 3$ nm as approximated from the experimental design of the stack. Taking $\epsilon = 9$ for the relative permittivity of MgO according to Ref. 2, we obtain $r = 0.2$ nm. This shows that the impurities involved in the transport are of atomic sizes and should indeed correspond to single carbon atoms or dimers trapped inside the MgO lattice.

Let us now approximate both the transport and environmental quantum dots as two spheres of radius r , separated by a distance d . The capacitance C of the system is approximately given by:

$$C = \frac{2\pi\epsilon_0\epsilon r}{1 - \frac{r}{d-r}}$$

According to the observed shift $\Delta_w = 70$ mV which shall be due to the change of charge of one environmental quantum dot by a quantum of elementary charge, we should then write:

$$e = C\Delta_w.$$

which leads to the distance between the dots:

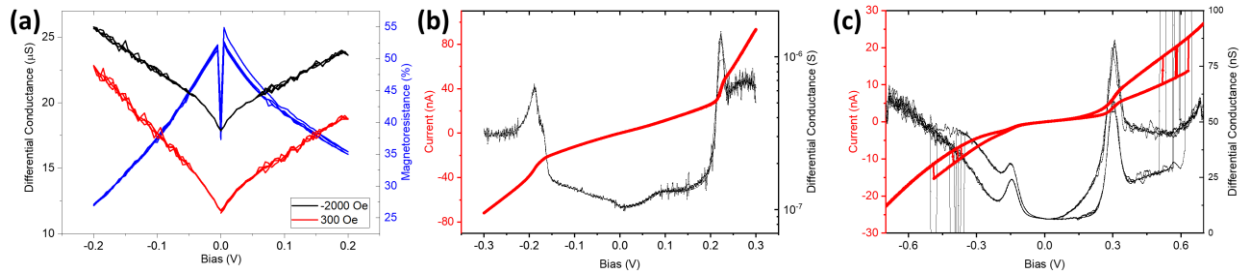
$$d = r \left(1 + \frac{1}{1 - \frac{2\pi\epsilon_0\epsilon r \Delta_w}{e}} \right).$$

With $r = 0.2$ nm as estimated above; we obtain the following approximation:

$$d \approx 2r ,$$

such as $d = 0.4$ nm. We thus find that the distance between the transport quantum dots and the environmental charging species is of the order of the diameter of the dots, so the control dot should be a second, third or fourth neighboring site of the transport dot in the MgO lattice. This estimation confirms that we are indeed observing the interaction of a reduced number of atomic formations closely packed inside the MgO barrier which are producing single-electron effects.

Note 6: Other junctions

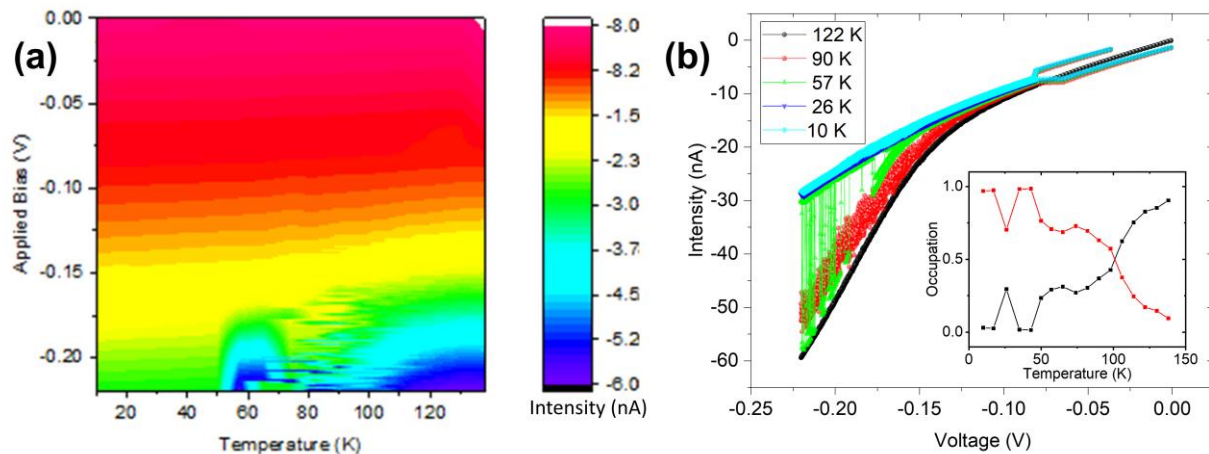


Suppl. Fig. S11: Magnetotransport experiments on other junctions. (a) Differential Conductance for the P (black) and AP (red) states and TMR (blue) plots at 10 K for junction F10. (b) and (c) Intensity-potential (black) and differential conductance (red) plots at 10 K and -2000 Oe for junctions B11 and B5 respectively.

Magnetoresistive properties have also been measured on several of these junctions, of the same kind as G10 and C5 presented in the main text. SI Fig.S11(a) shows that the electrical intensity of the junction F10 differs between the P and the AP configurations of the electrodes. This results in an apparent magnetoresistance of up to 60% that is maximal around 0. The conductance plot features two singular characteristics. First, the V-shaped spike around 0 mV, referred as the Zero-Bias anomaly (ZBA) [3-5], may indicate that an impurity state close to the Fermi level is located inside the MgO barrier [6]. This ZBA seems more pronounced in the P state than in the AP state as the deviation from linearity is more present at -2000 Oe in SI Fig.S11(a). Then, the noise visible in the linear part of the conductance, above 50 mV and below 50 mV should indicate the presence of two or more states close in energy which would result in several interfering nanotransport paths. An asymmetry is also observed in this figure: at negative bias the conductance is higher than at positive bias, in particular in the AP state which suggests that a structural asymmetry renders the electrodes nonequivalent. The drop in the junction resistance with increasing bias voltage is greater for antiparallel alignment of the magnetic electrodes than for parallel alignment which has been accounted for by spin excitations localized at the interfaces between the electrodes and the tunnel barrier [3].

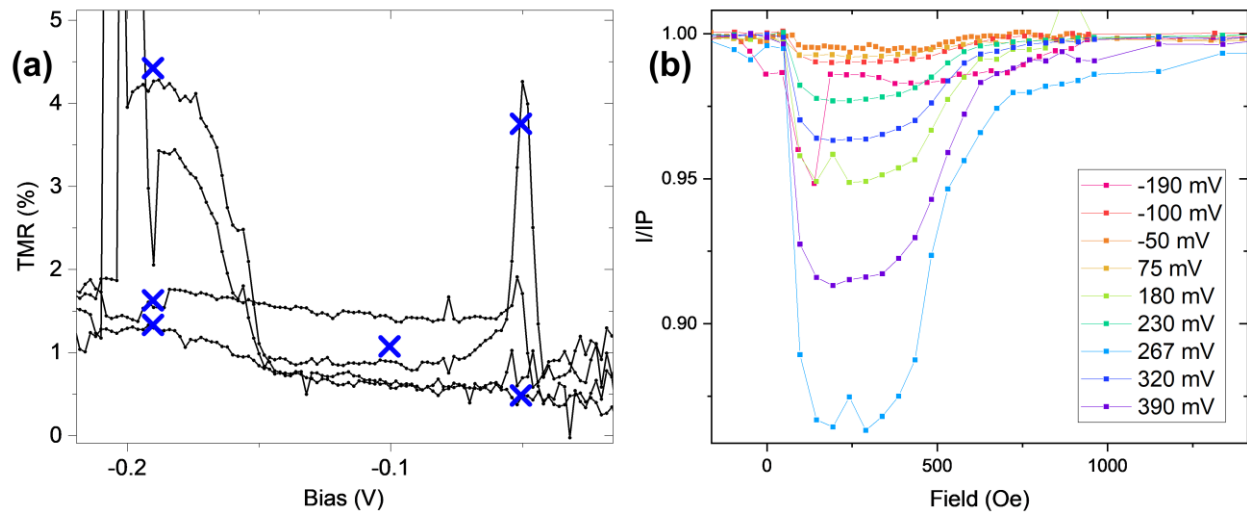
Of the 58 devices which have been tested, four other junctions displayed memristive behaviors, similar to G10 and C5, containing branch jumps and conductance peaks (see Figure SI Fig.S11(c)) which suggests the potential reproducibility of this phenomenon. Five other junctions also presented non-linear intensity-potential characteristics (see SI Fig.S11(b)) translating into sharp conductance peaks, but without branch jumps, looking more like standard MgO junctions without Carbon inside, but with a lower magnetoresistance.

Note 7: Memristance and temperature dependence



Suppl. Fig. S12: Temperature dependence of the memristive behavior. (a) Color plot of the current as a function of the temperature and applied bias for junction G10. (b) Intensity-Voltage characteristic of junction G10 recorded at five different temperatures. Inset: occupation probability of the low (in red) and high (in black) absolute intensity branches as a function of temperature.

Note 8: Magnetoresistance



Suppl. Fig. S13: **Magnetoresistance.** (a) Plot of the tunnel magnetoresistance as a function of the bias calculated from the intensity-voltage characteristic in the P and AP states of junction G10. The blue crosses represent points that have been confirmed by $I(H)$ experiments. The TMR enhancement due to the different memristive Coulomb blockade peaks can be observed. (b) Relative intensity compared to the P state as a function of the external field for different applied bias obtained from junction G10.

[1] A. M. Drews, M. Kowalik, and K. J. M. Bishop, "Charge and force on a conductive sphere between two parallel electrodes: A Stokesian dynamics approach," *Journal of Applied Physics* 116, 074903 (2014).

[2] D. R. Lide, G. Baysinger, S. Chemistry, L. I. Berger, R. N. Goldberg, and H. V. Kehiaian, "CRC Handbook of Chemistry and Physics".

[3] S. Zhang, P. M. Levy, A. C. Marley, and S. S. P. Parkin, "Quenching of Magnetoresistance by Hot Electrons in Magnetic Tunnel Junctions," *Physical Review Letters* 79, 3744–3747 (1997).

[4] A. F. G. Wyatt, "Anomalous Densities of States in Normal Tantalum and Niobium," *Physical Review Letters* 13, 401–404 (1964).

[5] J. A. Appelbaum and L. Y. L. Shen, "Zero-Bias-Conductance Peak Anomaly of Ta-I-Al Tunnel Junctions at 0.3 K and 90 kG," *Physical Review B* 5, 544–553 (1972).

[6] G.-X. Miao, M. Münzenberg, and J. S. Moodera, "Tunneling path toward spintronics," *Reports on Progress in Physics* 74, 036501 (2011).

[7] <https://lmfit.github.io/lmfit-py/>